

Solitary matter waves in combined linear and nonlinear potentials: Detection, stability, and dynamics

Scott Holmes

School of Physics and Astronomy, University of Birmingham, Birmingham, UK

Mason A. Porter*

Oxford Centre for Industrial and Applied Mathematics, Mathematical Institute, University of Oxford, Oxford OX1 3LB, UK

Peter Krüger

Midlands Ultracold Atom Research Centre, School of Physics & Astronomy, The University of Nottingham, Nottingham, UK

Panayotis G. Kevrekidis

Department of Mathematics and Statistics, University of Massachusetts, Amherst, Massachusetts 01003, USA

(Received 8 January 2013; revised manuscript received 15 June 2013; published 24 September 2013)

We study statically homogeneous Bose-Einstein condensates with spatially inhomogeneous interactions and outline an experimental realization of compensating linear and nonlinear potentials that can yield constant-density solutions. We illustrate how the presence of a step in the nonlinearity coefficient can only be revealed dynamically and examine how to reveal it by exploiting the inhomogeneity of the sound speed with a defect-dragging experiment. We conduct computational experiments and observe the spontaneous emergence of dark solitary waves. We use effective-potential theory to perform a detailed analytical investigation of the existence and stability of solitary waves in this setting, and we corroborate these results computationally using a Bogoliubov–de Gennes linear stability analysis. We find that dark solitary waves are unstable for all step widths, whereas bright solitary waves can become stable through a symmetry-breaking bifurcation as one varies the step width. Using phase-plane analysis, we illustrate the scenarios that permit this bifurcation and explore the dynamical outcomes of the interaction between the solitary wave and the step.

DOI: [10.1103/PhysRevA.88.033627](https://doi.org/10.1103/PhysRevA.88.033627)

PACS number(s): 03.75.-b, 05.45.Yv, 67.85.Hj

I. INTRODUCTION

For almost two decades, Bose-Einstein condensates (BECs) have provided a fruitful experimental, computational, and theoretical testbed for investigating nonlinear phenomena. In the mean-field limit, a BEC is governed by the Gross-Pitaevskii (GP) equation [1], which is a nonlinear Schrödinger (NLS) equation with an external potential. The NLS equation is important in many fields [2], and many ideas from disciplines such as nonlinear optics have proven important for investigations of BECs. Moreover, the ability to control various parameters in the GP equation makes it possible to create a wide range of nonlinear excitations, and phenomena such as bright [3,4], dark [5–7], and gap [8] solitary waves (and their multicomponent [9] and higher-dimensional [10,11] generalizations) have been studied in great detail using a variety of external potentials [10,11].

The GP equation's cubic nonlinearity arises from a BEC's interatomic interactions, which are characterized by the s -wave scattering length. The sign and magnitude of such interactions can be controlled using Feshbach resonances [12–14], and this has led to a wealth of interesting theoretical and experimental scenarios [3,4,15,16]. In a recent example, Feshbach resonances were used to induce spatial inhomogeneities in the scattering length in Yb BECs [17]. Such *collisional inhomogeneities*, which amount to placing a BEC in a nonlinear potential in addition to the usual linear

potential, can lead to effects that are absent in spatially uniform condensates [18–21]. This includes adiabatic compression of matter waves [22], enhancement of the transmission of matter waves through barriers [23], dynamical trapping of solitary waves [23], delocalization transitions of matter waves [24], and many other phenomena. Nonlinear potentials have also led to interesting insights in studies of photonic structures in optics [25].

In the present paper, we study the situation that arises when spatial inhomogeneities in nonlinear and linear potentials are tailored in such a way that they compensate each other to yield a constant-density solution of the GP equation. We demonstrate how to engineer this scenario in experiments and investigate it for a step-like configuration of the potentials. This situation is particularly interesting because the inhomogeneity is *not* mirrored in the BEC's density profile. Consequently, this situation is indistinguishable from one with homogeneous linear and nonlinear potentials when using *static* density measurements. We show that the step is, nevertheless, revealed *dynamically* in an impurity-dragging experiment [26], and we observe the emission of dark solitary waves when the dragging speed is above a critical velocity (which is different inside and outside of the step). This spontaneous emergence of solitary waves motivates their study as a dynamical entity in this setting. We use effective-potential theory to examine the existence and potential dynamical robustness of dark and bright quasi-one-dimensional (quasi-1D) solitary waves for various step-potential parameters. We find that dark solitary waves are always dynamically unstable as stationary states inside of the step, although the type of their instability

*porterm@maths.ox.ac.uk

depends on the step parameters. In contrast, bright solitary waves exhibit a symmetry-breaking bifurcation as the step width is increased, so we analyze their dynamics using a phase-plane description of their motion through the step. Our effective-potential picture not only unveils interesting bifurcation phenomena but also enables an understanding of the potential dynamical outcomes of the interaction of solitary waves with such steps.

In this paper, we highlight the fundamental difference between linear and nonlinear potentials in the dynamics of a quantum degenerate 1D Bose gas. In the static picture, one type of potential can be adjusted to completely compensate the other. However, the dynamical picture is different, as a flow of the Bose gas across inhomogeneities exhibits interesting dynamics. In the present investigation, we use step potentials to illustrate this phenomenon.

The remainder of this paper is organized as follows. In Sec. II, we present our model and its associated physical setup. In Sec. III, we discuss a proposal for an experimental implementation of compensating linear and nonlinear potentials. In Sec. IV, we discuss the problem of dragging a moving defect through the step and the ensuing spontaneous emergence of solitary waves. In Sec. V, we examine the existence, stability, and dynamics of the solitary waves both theoretically and computationally. Finally, we summarize our findings and propose several directions for future study in Sec. VI.

II. MODEL AND SETUP

We start with the three-dimensional (3D) time-dependent GP equation and consider a cigar-shaped condensate by averaging over the transverse directions to obtain a quasi-1D GP equation [1,10,11]. In performing the averaging, we assume that the BEC is strongly confined in the two transverse directions with a trapping frequency of ω_{\perp} [43]. The solution of the quasi-1D GP equation is a time-dependent macroscopic wave function $\Psi(z,t)$. We use the standing-wave ansatz $\Psi(z,t) = \phi(z)e^{-i\mu t}$ to obtain the time-independent GP equation

$$-\frac{1}{2}\phi_{zz} - \mu\phi + V_{\text{ext}}(z)\phi + g(z)|\phi|^2\phi = 0, \quad (1)$$

where ϕ is measured in units of $(2|a_0|)^{-1/2}$ and $g(z)$ is a spatially varying nonlinearity associated with the (rescaled) scattering length $a(z)$ via $g(z) = a(z)/|a_0|$. We measure length in units of $a_{\perp} \equiv \sqrt{\hbar/(m\omega_{\perp})}$ and time in units of ω_{\perp}^{-1} , where m is the mass of the atomic species in the condensate. The constant a_0 is the value of the scattering length in the associated collisionally homogeneous system. Equation (1) has two conserved quantities: the number of atoms $N = (a_{\perp}/[2|a_0|]) \int_{-\infty}^{+\infty} |\Psi|^2 dz$ and the Hamiltonian [11].

For a square-step linear potential, one can use the Thomas-Fermi approximation ($\phi_{zz} = 0$) for the ground state [11]. Equating the densities inside and outside of the step then gives the constraint

$$\gamma = \frac{\Delta V}{\Delta g} = \frac{V_0 - \mu}{g_0}, \quad (2)$$

where V_0 and g_0 are the constant background linear and nonlinear potentials, and ΔV and Δg are the differences

between the step and the background values of $V(z)$ and $g(z)$. The parameter γ thus measures (and balances) the relative strengths of the steps in the linear and nonlinear potentials. To preserve smoothness, we implement the steps using hyperbolic tangent functions:

$$\begin{aligned} V(z) &= V_0 + \Delta V(z) = V_0 + \frac{\Delta V}{2} [\tanh(z_+) - \tanh(z_-)], \\ g(z) &= g_0 + \Delta g(z) = g_0 + \frac{\Delta g}{2} [\tanh(z_+) - \tanh(z_-)], \end{aligned} \quad (3)$$

where $z_{\pm} = (z \pm z_0)/s$, the step width is $2z_0$, and s controls the sharpness of the step edges. From Eq. (2), it follows that $\Delta V = \gamma \Delta g$. For the remainder of this article, we take $V_0 = 0$ and $|g_0| = |\mu| = 1$. This yields $\gamma = -1$ and corresponds to nonlinear and linear steps of equal and opposite depths and heights. (The parameters μ and g_0 always have the same sign: $\mu < 0$ and $g_0 < 0$ for attractive BECs, and $\mu > 0$ and $g_0 > 0$ for repulsive BECs.)

III. PROPOSAL FOR EXPERIMENTAL IMPLEMENTATION

Techniques for manipulating cold quantum gases have become both advanced and accurate, and they allow experimentalists to form a variety of potentials with optical and/or magnetic fields, especially near microstructured atom chips [28,29]. It was shown recently that spatially varying nonlinear potentials, which have been of theoretical interest for several years [18–20], can be used to address a novel scenario that can also be implemented experimentally [17]. Straightforward implications of a spatial inhomogeneity in the coefficient g include static density variations as a result of the inhomogeneous mean field. To distinguish this type of effect from more subtle dynamical and beyond-mean-field phenomena, it is desirable to compensate linear and nonlinear contributions of the potential in such a way that the static density profile remains homogeneous (as would be the case if all potentials were homogeneous). In this section, we discuss how such a situation can be achieved experimentally. (In Sec. IV, we will give an example of a purely dynamical phenomenon that arises from it.)

A spatially varying magnetic field $B(z)$ results in a proportionally varying linear potential $V(z) = m_F g_F \mu_B B(z)$ for magnetic spin states (where the magnetic quantum number is m_F , the Landé factor is g_F , and the Bohr magneton is μ_B) at sufficiently low magnetic fields within the regime of validity of the linear Zeeman effect. For specific atomic species and spin states, there is an additional resonant dependence (a Feshbach resonance [30]) of g on the magnetic field,

$$g(B) = g_{\text{bg}} \left(1 - \frac{\Delta}{B - B_0} \right), \quad (4)$$

where g_{bg} is the background coupling constant, B_0 is the resonance field, and Δ is the resonance width. The condition of compensating linear and nonlinear potentials is fulfilled within the Thomas-Fermi approximation when

$$n \frac{\partial g}{\partial B} = - \frac{\partial V}{\partial B}. \quad (5)$$

In theory, this implies for any given density n that there is a field B_c near a resonance B_0 at which Eq. (5) is satisfied. Consequently, the density must remain constant for any static profile $B(z)$ as long as $B(z) - B_c$ is sufficiently small [so that $g(B)$ is an approximately linear function of B].

In practice, however, large nonlinearities lead to fast three-body recombination losses from traps and hence have to be avoided [30]. An atomic species with appropriate properties is cesium, for which the above conditions are fulfilled at typical densities of 10^{13} – 10^{14} cm $^{-3}$ for fields near the narrow Feshbach resonances at 19.8 and 53.5 G [31].

Optical dipole traps near the surface of atom chips [32] provide an environment in which magnetic fields can be accurately tuned to and varied about the critical magnetic field B_c at the above parameter values. One can bring the trap close to independent microstructures on the surface of a chip by coating the surface with a highly reflective layer so that a standing light wave forms a 1D optical lattice whose near-surface wells can be loaded with the atomic sample. Alternatively, one can focus a single laser beam on a position near the surface at a frequency that is slightly below that of the main atomic transition (i.e., one can red-detune it). In this case, integrated optics and microlenses might help to reduce the atom-surface distance d_{surf} to the single-micron regime. Once the trap is placed and populated with an atomic sample, currents that pass through appropriately shaped surface-mounted conductor patterns produce the necessary magnetic field profiles that we described above. The field-tailoring resolution and hence the width of a possible step are limited by d_{surf} . It is feasible to reduce this length to roughly 1 μm in current experiments. In particular, one can exploit the lattice approach [32], in which the closest wells form at $d_{\text{surf}} \approx \lambda$, where the wavelength λ is in the optical range (i.e., $\lambda \lesssim 1 \mu\text{m}$).

IV. DRAGGING A DEFECT THROUGH THE STEP

Using the above techniques, the effect of a step on the static density profile can be removed by construction. In this case, it is interesting to investigate if and how the density profile is modified when a step is moving relative to the gas. We show by performing computational experiments that the presence of steps in the linear and nonlinear potentials can be revealed by dragging a defect through the BEC [26,33]. For the linear and nonlinear steps that we described above, the condensate density is constant within and outside of the step. However, the speed of sound c is different in the two regions:

$$c = \sqrt{g(z)n(z)}, \quad (6)$$

where $n(z) = |\phi(z)|^2$ is the BEC density [34]. To perform computations that parallel viable experiments, we simulate a moving defect using a potential of the form

$$V(z,t) = A e^{-[z-r(t)]^2/w^2}, \quad (7)$$

where $r(t) = r(0) + vt$ represents the center of a defect that moves with speed v , and A and w are (respectively), amplitude- and width-related constants. The dynamics of defects moving in a BEC are sensitive to the speed of the defect relative to the speed of sound: speeds in excess of the speed of sound (i.e., supercritical defects) lead to the formation of dark solitary

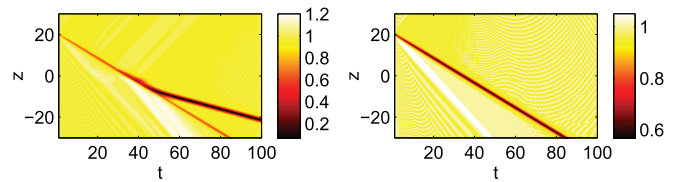


FIG. 1. (Color online) Numerical computations of defect dragging in the quasi-1D GP equation. Left: Emission of a dark solitary wave as a defect is dragged through a step. Right: The same computational experiment, but without a step (so there is no solitary-wave emission). The defect speed is $v = 0.6$, and the other parameter values are $\gamma = -1$ and $\Delta V = 0.5$.

waves traveling behind the defect, whereas speeds below the speed of sound (i.e., subcritical defects) do not [33].

There are three possible scenarios. First, when the speed is subcritical, there is a density depression with essentially the same functional form as the linear potential. This changes shape slightly in the presence of the step; it deepens and widens for a step with $\Delta g < 0$, and it becomes shallower and narrower when $\Delta g > 0$ [44]. When the speed is higher but still subcritical, the situation is similar—except that the depression distorts slightly, giving rise to a density hump in front of the defect. Second, when the defect speed is supercritical within the step region but subcritical outside of it, we expect the nucleation of dark solitary waves in the step region. Because the defect's speed is lower than the background sound speed, the emission of solitary waves downstream of the defect becomes a clear indication of the presence of a step. We demonstrate this scenario in Fig. 1. The third possible scenario involves a defect that is supercritical in both regions.

V. EXISTENCE, STABILITY, AND DYNAMICS OF SOLITARY WAVES

A. Theoretical analysis

Our scheme for applying compensating steps to the linear and nonlinear potentials and our ensuing observation that solitary waves emerge from moving steps warrant a detailed investigation of the dynamics in this scenario. In particular, we examine the existence and stability of solitary-wave solutions as a function of step parameters (especially step width).

1. Bogoliubov–de Gennes analysis

We apply the Bogoliubov–de Gennes (BdG) ansatz

$$\Psi(z,t) = e^{-i\mu t} \left\{ \phi_0(z) + \sum_j [u_j(z)e^{-i\omega_j t} + v_j^*(z)e^{i\omega_j t}] \right\} \quad (8)$$

to the time-dependent quasi-1D GP equation. Equation (8) defines the linear eigenfrequencies ω_j for small perturbations, which are characterized by eigenvectors $u_j(z)$ and $v_j(z)$. Linearizing the time-dependent GP equation about the reference state $\phi_0(z)$ using Equation (8) yields the BdG eigenvalue problem. The eigenfrequencies ω_j come in real (marginally stable) or imaginary (exponentially unstable) pairs or as complex (oscillatorily unstable) quartets.

In our analytical approach, we examine perturbations of the time-independent GP equation (1) with constant potentials

$V(z) \equiv V_0 = 0$ and $g(z) \equiv g_0 = \pm 1$. The perturbations in the linear and nonlinear steps are thus $\Delta g(z)$ and $\Delta V(z) = \gamma \Delta g(z)$. We introduce $\epsilon \equiv |\Delta g|$ as a small parameter and (to facilitate presentation) use the term “negative width” to describe a step with $\Delta g < 0$. When $g_0 = \pm 1$, Eq. (1) has two families of (stationary) soliton solutions, which are characterized by center position ξ and chemical potential μ . The case $g_0 = -1$ yields bright solitons,

$$\phi_{\text{bs}}(z - \xi) = \eta_{\text{bs}} \operatorname{sech}(\eta_{\text{bs}}(z - \xi)), \quad (9)$$

where $\eta_{\text{bs}} = \sqrt{-2\mu}$ and $\mu < 0$. The case $g_0 = 1$ yields dark solitons,

$$\phi_{\text{ds}}(z - \xi) = \eta_{\text{ds}} \tanh(\eta_{\text{ds}}(z - \xi)), \quad (10)$$

where $\eta_{\text{ds}} = \sqrt{\mu}$ and $\mu > 0$. Equations (9) and (10) represent, respectively, the stationary forms of the bright and dark soliton solutions.

2. Effective-potential theory

We use a Melnikov analysis to determine the persistence of bright [36] and dark solitary waves [37]. Stable (respectively, unstable) solitary waves exist at minima (respectively, maxima) of an effective potential M_{bs} . We find that bright solitary waves can, in principle, be stable within the step in the potentials. However, in contrast to bright solitary waves, stationary dark solitary waves are generically unstable within the step.

To determine the persistence of a bright solitary wave, we calculate when its center position induces its associated Melnikov function (i.e., its perturbed energy gradient) [36] to vanish. This yields the equation

$$M'_{\text{bs}}(\xi_0) = \int_{-\infty}^{\infty} \left[\frac{d[\Delta V(z)]}{dz} \phi_{\text{bs}}^2(z - \xi_0) + \frac{1}{2} \frac{d[\Delta g(z)]}{dz} \phi_{\text{bs}}^4(z - \xi_0) \right] dz = 0 \quad (11)$$

for the first derivative of the potential at the solitary-wave center $\xi = \xi_0$.

The GP equation without a potential is spatially homogeneous, and it possesses translational and U(1)-gauge symmetries. These symmetries are associated with a quartet of eigenfrequencies at the origin. When the translational symmetry is broken [e.g., by the steps in $V(z)$ and $g(z)$], a pair of eigenfrequencies leaves the origin. Tracking their evolution makes it possible to examine the stability of solitary waves of the perturbed system. We follow these eigenfrequencies by computing the function

$$M''_{\text{bs}}(\xi_0) = \int_{-\infty}^{\infty} \left[\frac{d^2[\Delta V(z)]}{dz^2} \phi_{\text{bs}}^2(z - \xi_0) + \frac{1}{2} \frac{d^2[\Delta g(z)]}{dz^2} \phi_{\text{bs}}^4(z - \xi_0) \right] dz, \quad (12)$$

which determines the concavity of the perturbed energy landscape and is directly associated with the eigenfrequencies of the linearization through [36]

$$\omega^2 = \frac{1}{2\sqrt{-2\mu}} M''_{\text{bs}}(\xi_0) + O(\epsilon^2), \quad (13)$$

where we note that $M''_{\text{bs}}(\xi_0) = O(\epsilon)$. Stable (respectively, unstable) solitary waves exist at minima (respectively, maxima) of the effective potential M_{bs} . Hence, bright solitary waves can, in principle, be stable within the step.

We compute analogous expressions for dark solitary waves, but the Melnikov function now needs to be renormalized due to the presence of a nonzero background density [37]. The first and second derivatives of the effective potential M_{ds} evaluated at the solitary-wave center $\xi = \xi_0$ are

$$M'_{\text{ds}}(\xi_0) = \int_{-\infty}^{\infty} \left[\frac{d[\Delta V(z)]}{dz} [\eta_{\text{ds}}^2 - \phi_{\text{ds}}^2(z - \xi_0)] + \frac{1}{2} \frac{d[\Delta g(z)]}{dz} [\eta_{\text{ds}}^4 - \phi_{\text{ds}}^4(z - \xi_0)] \right] dz = 0 \quad (14)$$

and

$$M''_{\text{ds}}(\xi_0) = \int_{-\infty}^{\infty} \left[\frac{d^2[\Delta V(z)]}{dz^2} [\eta_{\text{ds}}^2 - \phi_{\text{ds}}^2(z - \xi_0)] + \frac{1}{2} \frac{d^2[\Delta g(z)]}{dz^2} [\eta_{\text{ds}}^4 - \phi_{\text{ds}}^4(z - \xi_0)] \right] dz \neq 0. \quad (15)$$

The expression for the associated eigenfrequencies in this case is [37]

$$\omega^2 = \frac{1}{4} M''_{\text{ds}}(\xi_0) \left(1 - \frac{i\omega}{2} \right) + O(\epsilon^2), \quad (16)$$

where we choose the root that satisfies $\operatorname{Re}(i\omega) > 0$ and we note that $M''_{\text{ds}}(\xi_0) = O(\epsilon)$.

The main difference in the spectra for dark versus bright solitary waves is that the continuous spectrum associated with the former (due to the background state) lacks a gap about the origin. Consequently, exiting along the imaginary axis is not the only way for eigenfrequencies to become unstable. Even when eigenfrequencies exit toward the real axis, they immediately leave it as a result of their collision with the continuous spectrum; this leads to an eigenfrequency quartet. Thus, stationary dark solitary waves are generically unstable within the step.

3. Computational results

We identify solitary-wave solutions using a fixed-point iteration scheme, solve the BdG equations numerically to determine their corresponding eigenfrequencies, and employ parameter continuation to follow the solution branches as we vary the step width.

We start with the $\xi_0 = 0$ branch, which exists for all step widths. In Fig. 2, we show the development of the eigenfrequencies of this branch of solutions as a function of step width for both dark (left) and bright (right) solitary waves. We obtain good *quantitative* agreement between our results from effective-potential theory and those from BdG computations for the nonzero eigenfrequency associated with the intrinsic (translational) dynamics of the solitary wave.

For the case of repulsive BECs ($g > 0$), the branch of solutions at $\xi = 0$ has a real instability for $\Delta g < 0$ (i.e., $\Delta V > 0$) and an oscillatory instability for $\Delta g > 0$. We capture both types of instabilities accurately using effective-potential theory. An interesting but unphysical feature of the dark solitary waves is the presence of small “jumps” in the

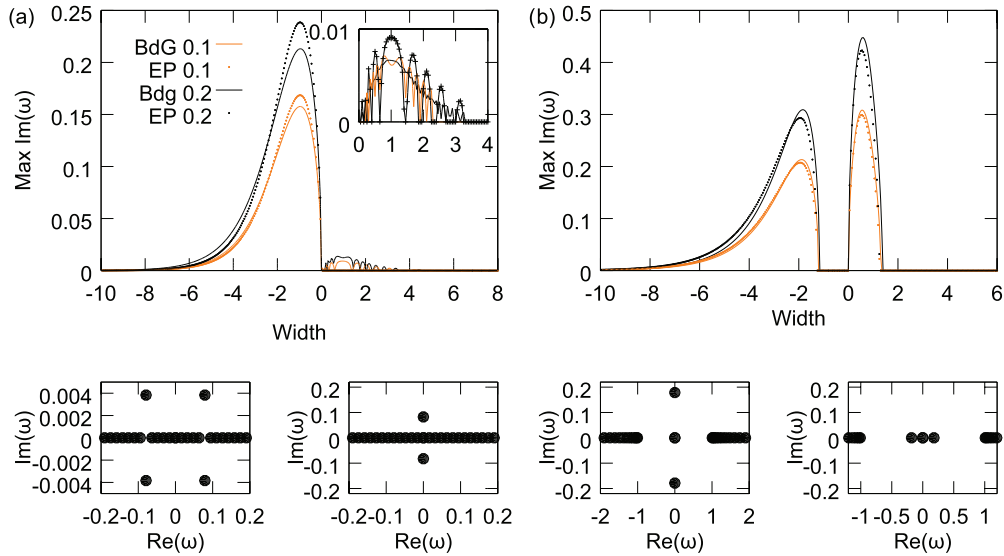


FIG. 2. (Color online) Top: Maximum imaginary eigenfrequencies versus step width (where a negative step width means that $\Delta g < 0$) for (left) dark solitary waves and (right) bright solitary waves. We show results for the perturbation strengths $\epsilon = |\Delta g| = 0.1$ and $\epsilon = 0.2$. Dotted curves represent results of analytical calculations from effective-potential (EP) theory, and solid curves represent numerical calculations using the BdG equations. The inset in the left panel shows finite-size effects (see the text). Bottom: Examples of the corresponding eigenfrequency spectra for $\epsilon = 0.1$. For both bright and dark solitary waves, we show the spectrum for a step width of $2z_0 = 0.25$ in the left panels and for a step width of $2z_0 = -0.25$ in the right panels.

eigenfrequencies. These jumps are finite-size effects that arise from the discrete numerical approximation to the model's continuous spectrum [38].

The case of attractive BECs ($g < 0$) is especially interesting. A pitchfork (symmetry-breaking) bifurcation occurs as the step widens; it is supercritical for $\Delta g < 0$ and subcritical for $\Delta g > 0$. In this case, oscillatory instabilities are not possible when translational invariance is broken [36]. A direct and experimentally observable consequence of our analysis is that (for $\Delta g > 0$) bright solitary waves remain stable for sufficiently large step widths, whereas narrowing the step should eventually lead to unstable dynamics. For dark solitary waves, by contrast, we expect the dynamics to be unstable in experiments for all step widths. However, as illustrated in the top left panel of Fig. 2, the instability growth rates are rather different for $\Delta g > 0$ and $\Delta g < 0$.

To further probe the bifurcation, we study the Newtonian dynamics [39] of the bright solitary wave,

$$m_{\text{eff}} \frac{d^2 \xi}{dt^2} = -\nabla U(\xi) = 2M'_{\text{bs}}(\xi)/N, \quad (17)$$

where the effective mass is $m_{\text{eff}} = 1/2$. We examine phase portraits of Eq. (17) by plotting the center-of-mass position $z_{\text{cm}} \approx \xi$ versus the center-of-mass velocity $v_{\text{cm}} \approx \frac{d\xi}{dt}$. As we illustrate in Fig. 3, this is convenient for examining changes in the dynamics as we alter the step width. For narrow steps (e.g., a width of $2z_0 = -1$), there is a center at $z_{\text{cm}} = 0$ that straddles two saddle points (stars) just outside of the step (whose edges we indicate using dash-dotted lines). When $\Delta g < 0$ (i.e., $\Delta V > 0$), a supercritical pitchfork bifurcation occurs at $2z_0 \approx -1.2$, as the center at the origin transitions to a pair of centers separated by a saddle at the origin

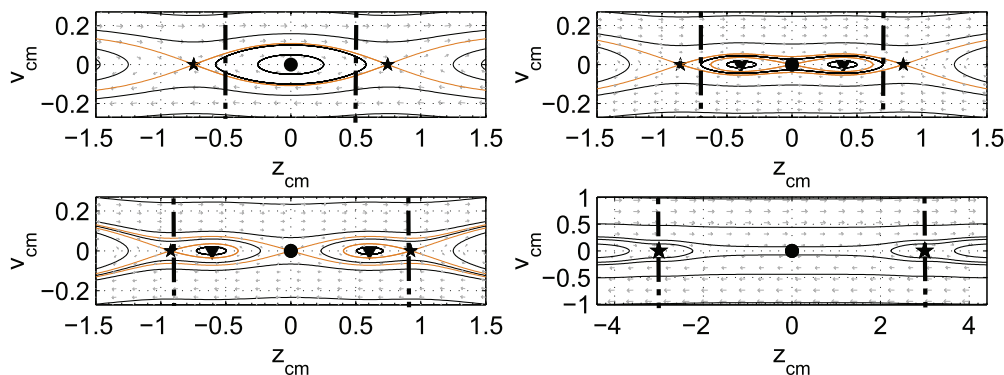


FIG. 3. (Color online) Phase planes for Newtonian dynamics that describe bright solitary waves in an attractive BEC for four different step widths. The thick dash-dotted lines represent the edges of the step. We highlight the equilibria with dots, triangles, and stars. The light (orange) curves correspond to trajectories that originate at equilibria, and we show other example trajectories as dark (black) curves. The step widths are (upper left) $2z_0 = -1$, (upper right) $2z_0 = -1.4$, (lower left) $2z_0 = -1.8$, and (lower right) $2z_0 = -6$.

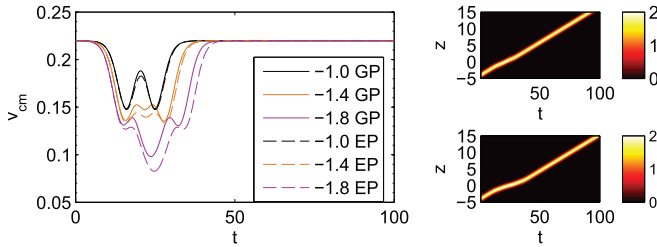


FIG. 4. (Color online) (Left) Effect of the step on the movement of a bright solitary wave for three different step widths for the GP equation (solid curves) and for numerical solutions of the Newtonian dynamics of the effective-potential (EP) equations (dashed curves). (Right) Contour plots of $|\psi(z,t)|^2$ obtained by solving the GP equation numerically for step widths of (top) -1 and (bottom) -1.8 .

(see the top-right panel). As the step widens further (bottom-left panel), the heteroclinic orbit that previously enclosed the central three equilibria is no longer present, and the centers are now surrounded by homoclinic orbits that emanate from the outer saddle points. Eventually (in particular, asymptotically), each outer saddle and its associated center annihilate one another (bottom-right panel). When $\Delta g > 0$, the types of equilibria are interchanged (saddles become centers, and vice versa). The main difference that occurs in this case is that solitary waves can no longer be reflected by the step. As one increases the magnitude of the step width from 0, there is a saddle flanked by two centers. At the bifurcation point, the central saddle splits into two saddles with a center between them.

The trajectories in phase space at different parameter values suggest a viable way to investigate the bifurcation experimentally (and hence to distinguish between narrow and wide steps). The presence of a step alters the path of a moving solitary wave, as is particularly evident by examining the wave speed. As we illustrate in Fig. 4, the solitary-wave dynamics depend on the number and type of phase-plane equilibria (and hence on the step width). The left panel shows how one can use variations in v_{cm} of a transmitted bright solitary wave to identify which equilibria are present (because each local extremum in the associated temporal evolution arises from the presence of an equilibrium point). The center-of-mass motion of the solitary wave is a particularly useful quantity, as it is directly accessible to experimental measurement through time-resolved detection of spatial density profiles. The technique outlined above for shaping the nonlinear potential—i.e., engineering the spatial profile $g(x)$ while automatically compensating it using the linear potential $V(x)$ —gives a straightforward method for adjusting the step width in the laboratory.

We examine trajectories starting from the same initial conditions, $(z_{\text{cm}}(0), v_{\text{cm}}(0)) = (4, -0.22)$, for step widths of -1 , -1.4 , and -1.8 . The simplest trajectory occurs for the narrowest width ($2z_0 = -1$): as the solitary wave traverses the step, its speed first drops before rising again in the center of the step and then dropping again as it leaves the step (due to its encounter with the two saddles and the center in the phase plane; see Fig. 3). For wider steps, the dynamics illustrate the effects of the bifurcation: instead of a single peak in the speed, there are now two peaks separated by a well. As the step widens further, the two peaks move outward and follow the centers to

the edge of the step. The maximum and minimum in each pair move closer together in both v_{cm} and t as one approaches the edge of the step. The solitary wave can be either transmitted (as illustrated in Fig. 4) or reflected by the step.

VI. CONCLUSIONS

We have introduced an experimentally realizable setup to study statically homogeneous BECs in mutually compensating inhomogeneous linear and nonlinear potentials. We have shown that—in contrast to the straightforward static scenario—a flowing gas will encounter sound-speed differences, which can induce interesting dynamics such as solitary-wave formation and motion. As a simple demonstration, we have examined a step defect, whose width affects the system’s dynamics. We conducted a thorough examination of solitary-wave stability and dynamics in this collisionally inhomogeneous setting. We also showed how to experimentally produce balancing linear and nonlinear potentials that yield constant-density solutions in the static case.

We found that effective-potential theory gives a good *quantitative* description of the existence and eigenfrequencies of both bright and dark solitary waves, and we used it to quantitatively track the evolution of the translational eigenfrequencies as a function of the step width. We identified a symmetry-breaking bifurcation in the case of attractive BECs and illustrated how the presence of the bifurcation is revealed by the motion of solitary waves through the step region. We also found that stationary dark solitary waves are generically unstable through either exponential or oscillatory instabilities.

The system that we have studied provides a promising setup for future investigations, as it allows the experimentally realizable possibility of solitary-wave control via accurate, independent tailoring of linear and nonlinear potentials. It would also be interesting to explore the phase-coherence properties of a collisionally inhomogeneous 1D quasicondensate, for which phase correlations (at zero temperature) decay algebraically with an interaction-dependent exponent [40]. Quasicondensates have comparatively small density fluctuations [41]. In contrast to the scenario on which we have focused in the present paper, even a static quasicondensate gas would reveal a step in the nonlinearity in an interference experiment [42] when the density profile is homogeneous. The study of such quasicondensates and their phase fluctuations is a topic of considerable current interest [41], and it is desirable to enhance our understanding of the properties of solitary waves in such systems.

ACKNOWLEDGMENTS

P.G.K. acknowledges support from the U.S. National Science Foundation (Grant No. DMS-0806762), the Alexander von Humboldt Foundation, and the Binational Science Foundation (Grant No. 2010239). P.K. thanks the EPSRC and the EU for support. P.G.K. and P.K. are grateful to Markus Oberthaler and the KIP of the University of Heidelberg and to Peter Schmelcher and the ZOQ of the University of Hamburg for their hospitality while this work was in progress. We also thank an anonymous referee for helpful comments. S.H. began his work on this project at University of Oxford.

- [1] C. J. Pethick and H. Smith, *Bose-Einstein Condensation in Dilute Gases*, 2nd ed. (Cambridge University Press, Cambridge, 2008).
- [2] C. Sulem and P. L. Sulem, *The Nonlinear Schrödinger Equation: Self-Focusing and Wave Collapse* (Spring-Verlag, New York, 1999).
- [3] K. E. Strecker, G. B. Partridge, A. G. Truscott, and R. G. Hulet, *Nature* **417**, 150 (2002).
- [4] S. L. Cornish, S. T. Thompson, and C. E. Wieman, *Phys. Rev. Lett.* **96**, 170401 (2006).
- [5] A. Weller, J. P. Ronzheimer, C. Gross, J. Esteve, M. K. Oberthaler, D. J. Frantzeskakis, G. Theocharis, and P. G. Kevrekidis, *Phys. Rev. Lett.* **101**, 130401 (2008); G. Theocharis, A. Weller, J. P. Ronzheimer, C. Gross, M. K. Oberthaler, P. G. Kevrekidis, and D. J. Frantzeskakis, *Phys. Rev. A* **81**, 063604 (2010).
- [6] I. Shomroni, E. Lahoud, S. Levy, and J. Steinhauer, *Nature Phys.* **5**, 193 (2009).
- [7] M. Baumert, E.-M. Richter, J. Kronjäger, K. Bongs, and K. Sengstock, *Nature Phys.* **4**, 496 (2008); S. Stellmer, C. Becker, P. Soltan-Panahi, E.-M. Richter, S. Dörscher, M. Baumert, J. Kronjäger, K. Bongs, and K. Sengstock, *Phys. Rev. Lett.* **101**, 120406 (2008).
- [8] B. Eiermann, Th. Anker, M. Albiez, M. Taglieber, P. Treutlein, K.-P. Marzlin, and M. K. Oberthaler, *Phys. Rev. Lett.* **92**, 230401 (2004).
- [9] D. Yan, J. J. Chang, C. Hamner, P. G. Kevrekidis, P. Engels, V. Achilleos, D. J. Frantzeskakis, R. Carretero-González, and P. Schmelcher, *Phys. Rev. A* **84**, 053630 (2011); M. A. Hoefer, J. J. Chang, C. Hamner, and P. Engels, *ibid.* **84**, 041605 (2011).
- [10] P. G. Kevrekidis, D. J. Frantzeskakis, and R. Carretero-González (eds.), *Emergent Nonlinear Phenomena in Bose-Einstein Condensates. Theory and Experiment* (Springer-Verlag, Berlin, 2008).
- [11] R. Carretero-González, D. J. Frantzeskakis, and P. G. Kevrekidis, *Nonlinearity* **21**, R139 (2008).
- [12] T. Köhler, K. Goral, and P. S. Julienne, *Rev. Mod. Phys.* **78**, 1311 (2006).
- [13] S. Inouye, M. R. Andrews, J. Stenger, H. J. Miesner, D. M. Stamper-Kurn, and W. Ketterle, *Nature* **392**, 151 (1998); S. L. Cornish, N. R. Claussen, J. L. Roberts, E. A. Cornell, and C. E. Wieman, *Phys. Rev. Lett.* **85**, 1795 (2000).
- [14] F. K. Fatemi, K. M. Jones, and P. D. Lett, *Phys. Rev. Lett.* **85**, 4462 (2000); M. Theis, G. Thalhammer, K. Winkler, M. Hellwig, G. Ruff, R. Grimm, and J. H. Denschlag, *ibid.* **93**, 123001 (2004).
- [15] J. Herbig, T. Kraemer, M. Mark, T. Weber, C. Chin, H. C. Nagerl, and R. Grimm, *Science* **301**, 1510 (2003); C. A. Regal, C. Ticknor, J. L. Bohn, and D. S. Jin, *Nature* **424**, 47 (2003); M. Bartenstein, A. Altmeyer, S. Riedl, S. Jochim, C. Chin, J. H. Denschlag, and R. Grimm, *Phys. Rev. Lett.* **92**, 203201 (2004).
- [16] H. Saito and M. Ueda, *Phys. Rev. Lett.* **90**, 040403 (2003); G. D. Montesinos, V. M. Pérez-García, and P. J. Torres, *Physica D* **191**, 193 (2004); M. Matuszewski, E. Infeld, B. A. Malomed, and M. Trippenbach, *Phys. Rev. Lett.* **95**, 050403 (2005).
- [17] R. Yamazaki, S. Taie, S. Sugawa, and Y. Takahashi, *Phys. Rev. Lett.* **105**, 050405 (2010).
- [18] P. Niarchou, G. Theocharis, P. G. Kevrekidis, P. Schmelcher, and D. J. Frantzeskakis, *Phys. Rev. A* **76**, 023615 (2007); F. Kh. Abdullaev and J. Garnier, *ibid.* **72**, 061605(R) (2005); F. Kh. Abdullaev, A. Abdumalikov and R. Galimzyanov, *Phys. Lett. A* **367**, 149 (2007); A. V. Carpentier, H. Michinel, M. I. Rodas-Verde, and V. M. Pérez-García, *Phys. Rev. A* **74**, 013619 (2006); V. M. Pérez-García, arXiv:nlin/0612028.
- [19] C. Wang, K. J. H. Law, P. G. Kevrekidis, and M. A. Porter, *Phys. Rev. A* **87**, 023621 (2013).
- [20] Y. V. Kartashov, B. A. Malomed, and L. Torner, *Rev. Mod. Phys.* **83**, 247 (2011).
- [21] A. S. Rodrigues, P. G. Kevrekidis, M. A. Porter, D. J. Frantzeskakis, P. Schmelcher, and A. R. Bishop, *Phys. Rev. A* **78**, 013611 (2008).
- [22] G. Theocharis, P. Schmelcher, P. G. Kevrekidis, and D. J. Frantzeskakis, *Phys. Rev. A* **72**, 033614 (2005).
- [23] G. Theocharis, P. Schmelcher, P. G. Kevrekidis, and D. J. Frantzeskakis, *Phys. Rev. A* **74**, 053614 (2006).
- [24] Yu. V. Bludov, V. A. Brazhnyi, and V. V. Konotop, *Phys. Rev. A* **76**, 023603 (2007).
- [25] Y. Kominis, *Phys. Rev. E* **73**, 066619 (2006); Y. Kominis and K. Hizanidis, *Opt. Express* **16**, 12124 (2008).
- [26] T. W. Neely, E. C. Samson, A. S. Bradley, M. J. Davis, and B. P. Anderson, *Phys. Rev. Lett.* **104**, 160401 (2010).
- [27] L. Salasnich, A. Parola, and L. Reatto, *Phys. Rev. A* **64**, 023601 (2001); A. Muñoz Mateo and V. Delgado, *ibid.* **77**, 013617 (2008).
- [28] R. Folman, P. Krüger, J. Denschlag, J. Schmiedmayer, and C. Henkel, *Adv. At. Mol. Opt. Phys.* **48**, 263 (2002).
- [29] G. Sinuco-León, B. Kaczmarek, P. Krüger, and T. M. Fromhold, *Phys. Rev. A* **83**, 021401(R) (2011).
- [30] C. Chin, R. Grimm, P. Julienne, and E. Tiesinaga, *Rev. Mod. Phys.* **82**, 1225 (2010).
- [31] C. Chin, V. Vuletić, A. J. Kerman, S. Chu, E. Tiesinga, P. J. Leo, and C. J. Williams, *Phys. Rev. A* **70**, 032701 (2004).
- [32] D. Gallego *et al.*, *Opt. Lett.* **34**, 3463 (2009).
- [33] V. Hakim, *Phys. Rev. E* **55**, 2835 (1997).
- [34] M. R. Andrews, D. M. Kurn, H.-J. Miesner, D. S. Durfee, C. G. Townsend, S. Inouye, and W. Ketterle, *Phys. Rev. Lett.* **79**, 553 (1997).
- [35] M. A. Hoefer, M. J. Ablowitz, I. Coddington, E. A. Cornell, P. Engels, and V. Schweikhard, *Phys. Rev. A* **74**, 023623 (2006).
- [36] T. Kapitula, P. G. Kevrekidis, and B. Sandstede, *Physica D* **195**, 263 (2004).
- [37] D. E. Pelinovsky and P. G. Kevrekidis, *Z. Angew. Math. Phys.* **59**, 559 (2008).
- [38] M. Johansson and Y. S. Kivshar, *Phys. Rev. Lett.* **82**, 85 (1999).
- [39] J. Fröhlich, S. Gustafson, B. L. G. Jonsson, and I. M. Sigal, *Commun. Math. Phys.* **250**, 613 (2004).
- [40] F. D. M. Haldane, *Phys. Rev. Lett.* **47**, 1840 (1981).
- [41] M. C. Garrett, T. M. Wright, and M. J. Davis, *Phys. Rev. A* **87**, 063611 (2013).
- [42] P. Krüger, S. Hofferberth, I. E. Mazets, I. Lesanovsky, and J. Schmiedmayer, *Phys. Rev. Lett.* **105**, 265302 (2010).
- [43] Our considerations can be extended to more accurate quasi-1D models [27], but we employ the quasi-1D GP setting for simplicity.
- [44] Additionally, initialization of the moving step or an impact on the step produces low-amplitude, oscillatory Hamiltonian shock waves [35].